AMMUNITION GROUP
PICATINNY ARSENAL
DOVER, NEW JERSEY

TECHNICAL SERVICES LABORATORY

METALS ENGINEERING SECTION

TECHNICAL MEMORANDUM
NO. ME-1-62

EVALUATION OF OXIDATION-RESISTANT COATINGS IN A WATER-STABILIZED ELECTRIC ARC AT TEMPERATURES TO 2325°C (4215°F)

BY
DOMENIC J. MOLELLA

MAY 1962

TECHNICAL MEMORANDUM NO. ME-1-62

EVALUATION OF OXIDATION-RESISTANT COATINGS IN A WATER-STABILIZED ELECTRIC ARC AT TEMPERATURES TO 2325°C (4215°)

by

D. J. MOLELLA

Reviewed by: W. H. Schoeller

W. H. Schoeller, Chief
Metals Engineering Lab. Section

H. H. Bronson

H. H. Bronson, Chief
Metallurgical Engineering Lab. Unit

Approved by: Karl G. Ottoson

Karl G. Ottoson
Chief, Technical Services

FORWARD

This report is transmitted for information only. It represents information that is subject to modification and/or withdrawal. The conclusions presented in this Technical Memorandum are those of the Technical Services Laboratory and should not be considered as bearing official Ordnance Corps approval, either explicit or implied.

TABLE OF CONTENTS

SECTION		PAGE
I.	Abstract	1
II.	Introduction	1
III.	Symbols	2
IV.	Apparatus andExperimental Procedure	2
V.	Results and Discussion	5
VI.	Table 1. Optical Pyrometer and Motion Picture Observation of Probes During Electric Arc Heat Tests	5
VII.	Conclusions	8
VIII.	References	9
IX.	Figures 1 through 19	10

TITLE:

Evaluation of Oxidation-Resistant Coatings in a Water-Stabilized Electric Arc at Temperatures to 2325° C (4215°F)

By Domenic J. Molella
Picatinny Arsenal, Dover, New Jersey

ABSTRACT:

Twelve oxidation-resistant coatings on molybdenum and graphite pressure sensing probe models were evaluated. These evaluations were made in an atmosphere simulating re-entry trajectory heating conditions experienced at a Mach No. of 8.5. A water-stabilized electric arc was used to simulate heat input of 450 BTU/ft^2-sec. to be reached in 25 seconds. Duration of test was 60 seconds.

Under conditions of equal heat input, the surface temperatures of the probes, as observed with a calibrated optical pyrometer, varied due to differences in the physical and thermodynamic properties of the coatings. The highest surface temperature, 2325°C (4215°F), was attained by a molybdenum probe with a zirconium diboride coating.

Out of nine coatings tested on molybdenum, a flame-sprayed coating of 90%W and 10% Z_rO_2 exhibited the least damage. Other coatings, Al-Cr-Si, $MoSi_2$, gradated Z_rO_2 and Z_rB_2 protected the molybdenum against catastrophic oxidation.

Out of three coatings tested on graphite, a vapor-deposited, silicon carbide coating showed the least damage. American Lava Corp proprietary coating and a 90% W and 10% Z_rO_2, flame-sprayed coating eroded but still protected the graphite against catastrophic oxidation.

INTRODUTION:

The probe configuration evaluated was that which was proposed for possible use on a theoretical Mach 8.5 missile. The pressure sensing probe system must have the capability of measuring total and static pressure for velocity determination. From the known velocity, the maximum allowable movement of the aerodynamic control surfaces are determined so that the maneuvering "G" limits of the missile are not exceeded. The probe also performs certain warhead functions.

Numerous experimental probes were subjected to wind tunnel and simulated flight tests in order to determine the most suitable aerodynamic design for this probe. In this design aerodynamic heating must also be considered since the maximum Mach number will be 8.5. When such Mach numbers are involved, it is customary to ascertain the trajectory that yields the greatest aerodynamic missile heat input and then design the system to meet the heat requirements of this trajectory. Such a trajectory is called the "Thermodynamic Design Trajectory".

From this design trajectory, which results in maximum heating, heat fluxes expected at the forward portion of the probes to be tested were determined (1) These flux calculations were based on the assumption of a cold wall. Since it was known that the flow field of the electric arc was subsonic, the flow away from the stagnation point would not be similar to that which exists when supersonic flow is present on the probe during flight. However, the flow at the stagnation point in the arc subsonic flow field was similar to the flow field present on the probe during flight. From these assumptions and calculations a heat flux vs time testing program on the probe models was proposed, as follows:

initial input - 65 BTU/ft^2-sec
maximum input - 450 BTU/ft^2-sec to be reached in 25 seconds
final input - 225 BTU/ft^2-sec at the end of 60 seconds

If a probe material or a material with a protective coating could withstand the maximum service heat inputs without ablating, oxidizing, burning or softening, the probe geometric configuration would be maintained throughout the trajectory and the probe would then perform its functions satisfactorily. In order to assure maintenance of the geometric configuration, only materials having high thermal conductivities, heat capacities and mechanical strengths at low and elevated temperatures should be considered. In the final selection of the best material, availability, fabricability and cost of the material should also be considered. This investigation was conducted to evaluate various materials and coatings to find a suitable combination to fulfill the above requirements.

Since a water stabilized electric arc can simulate the heat flux vs time that are obtained from the maximum trajectory, this apparatus was used for determining the most suitable probe material.

SYMBOLS:

Mo	molybdenum
90W+10ZrO_2	90% tungsten + 10% zirconia
Ti	titanium
Al-Cr-Si	aluminum-chromium-silicon
$MoSi_2$	molybdenum disilicide
ZrB_2	zirconium diboride
Si C	Silicon carbide

APPARATUS AND EXPERIMENTAL PROCEDURE:

HEAT TESTS:

A water-stabilized electric arc was used in the evaluation of the materials for resistance to high temperature gas flow. The arc operates in the vortex formed by a rapidly swirling body of water. Extremely high temperatures up to 25,000°F and high heat inputs (2500 BTU/ft^2-sec) are developed due to the increased current density arising from the restricted cross sectional area of the vortex and the cooling of the outer arc regions, which forces most of the current to flow in the center (2). The arc is struck in a vortex of water

between a ½" dia graphite disk with a 3/16" dia hole in the center as the cathode. The cathode is mounted in a water-cooled horizontal metal plate at ground potential, while the anode is vertically held by a collet directly below the cathode cavity. Figure 1 shows a schematic diagram of this apparatus. A lucite "swirl chamber" surrounds the anode. During operation water is introduced tangentially into the chamber at 36 psi and forms the vortex in which the arc burns.

The power supply for the arc consists of four welding generators connected in series. For stable operation about one half of the power is dissipated by a ballast resistor connected in series with the arc. Constant arc voltage is maintained by controlling a hydraulic mechanism which feeds the lower electrode at the proper rate by means of a voltage sensing device connected across the arc. Under these conditions, a power dissipation of 33kW results at the arc. A water-cooled parabolic cathode nozzle was developed for testing the probes in order to provide optimum reproducibility in the arc environment.

The models were mounted on an adjustable support and positioned so that when swung into the arc, the heat flux on the model simulated approximately the heat flux expected within a second or so of zero time (missile at rest). Figure 2 shows the water-stabilized electric arc apparatus before operation or prior to swinging the model into the jet. The power was then turned on and the arc flow field was set to the same voltage and amperage that was used to determine the steady temperature that would occur on the probe tip vs distance from the nozzle exit. These calibrations were previously made by using a black body (graphite) probe. When stable arc operation was attained, the probe model was positioned in the flow field. It was then moved axially towards the arc nozzle so that the heat flux vs time simulated the thermodynamic design trajectory and so that the maximum heat flux input (450 BTU/ft^2-sec) on the model occurred at 25 seconds. Figure 3 shows the electric arc in operation with a model under test.

High speed color motion pictures were made of the entire test run to show the heat input effects on the models.

PROBE MODELS:

The materials selected for evaluation on the models were based on current availability and fabricability and were also based on the results of a previous investigation of available high temperature materials (3). The materials and coatings selected to the probe configurations (Figure 4) at Picatinny Arsenal. The models had a concave nose-cylinder geometric shape with a pressure cavity at the nose. These to be coated were sent to private concerns for application of the various oxidation-resistant coatings. Identical coatings were also applied to flat specimens so that the characteristics of the coatings on the models prior to the heat tests could be determined. All of the coated and uncoated models and the coated flat specimens were ground to a RMS-16 surface finish.

Some of the coatings, listed below, were proprietary; therefore, very little was known about their compositions.

W-2 - Chromalloy Corp vapor-deposited coating on molybdenum believed to consist mostly of chromium along with some aluminum and silicon.

DURAK-MG - Chromizing Corp coating believed to be similar to the W-2 coating.

LM-5 - Linde Co flame-sprayed, modified molybdenum disilicide coating on molybdenum with additions of chromium carbide and aluminum.

Gradated Zirconia - Linde Co flame-sprayed, multi-layer coating on molybdenum consisting of a metal-rich+ zirconia undercoat and zirconia-rich+metal overcoat.

Am. Lava - American Lava Corp coating on graphite believed to consist of tungsten and silicon carbide.

SURFACE TEMPERATURE DETERMINATIONS:

A calibrated optical pyrometer was used to determine the highest surface temperature that was attained by each model during the electric arc heat test. The time (seconds) when this maximum temperature was reached was recorded.

Caution must be exercised in interpreting the optical pyrometer observations (4). The pyrometer measures a luminescence temperature, T_S, which is related to the true temperature, T, by the equation, as follows:

$$\frac{1}{T} - \frac{1}{T_S} = \frac{\lambda \log_e \epsilon_\lambda}{C_2}$$

where ϵ_λ is the spectral emissivity at wave length, λ (microns) and C_2 is the constant in the Wien equation for distribution of energy in the spectrum and has a value of 1.438 cm degrees. It was decided that correcting the optical pyrometer readings for emissivity differences was unnecessary since the same heat input flow field was repeated for each heat test and therefore, subjected the probes to the maximum heating trajectory. Also, little or no data were available on the emissivities of the various coatings and base materials used

METALLURGICAL EXAMINATIONS:

Visual examinations were made on the models before and after subjecting them to the arc heat tests in order to determine the extent of damage, if any, to the surfaces. The naked eye and standard low power (below 10X) optical magnifiers were used for these inspections. Still photographs were taken before and after heat testing the models

Microscopic examinations were conducted on the flat specimens to determine the metallurgical characteristics of the coating before the arc tests. Microscopic examinations were also conducted on all the models after the heat tests to determine the effects of the heat inputs. These examinations were made at magnifications up to 1000 times on polished specimens cut from the flat sheets

and at the nose portions of the probes. Standard metallographic procedures and microscopes were used. Photomicrographs showing the heat effects on the coatings and base materials were taken.

RESULTS AND DISCUSSION:

WATER-STABILIZED ELECTRIC ARC TESTS:

Descriptions of the various materials and coatings used on the probe models and the heat effects on them are shown in Table 1. These effects were determined by viewing color motion pictures of the models taken during the electric arc tests. Also included in the table are the maximum surface temperatures attained by the models, as determined with a calibrated optical pyrometer, and the time (seconds) to reach these temperatures.

TABLE 1. Optical Pyrometer and Motion Picture Observation of Probes During Electric Arc Heat Tests

Probe Material	Max Observed Temp (°C)	Time to Reach Max Temp (sec)	Color Motion Picture Observations
Mo with 90W+10Z_rO_2	2030	35	Excellent preservation of probe tip contour throughout test
Mo with Al-Cr-Si flame-sprayed coating, .010" thick	1790	35	Excellent preservation of probe tip contour throughout test
Mo with gradated Zirconia flame-sprayed coating, .015" thick	2180	40	Flaking started immediately but protection was very good
Mo with flame-sprayed Z_rB_2 coating, .010" thick	2325	40	Coating flaked at 15 sec. Slight erosion and oxidation apparent at 35 sec.
Mo + .5 Ti with $MoSi_2$ vapor-deposited coating, .0014" thick	1970	35	Excellent preservation of probe tip contour throughout test
Mo with $MoSi_2$ vapor-deposited coating, .0014" thick	2155	35	Coating failed at 20 sec. Erosion and oxidation apparent

TABLE 1. (Continued)

Probe Material	Max Observed Temp. (°C)	Time to Reach Max Temp (sec)	Color Motion Picture Observations
Mo with DURAK-MG vapor-deposited coating, .0014" thick	2120	55	Coating failure at 34 sec. Leading edge exposed at 40 sec.
Mo with DURAK-MG vapor-deposited coating, .0014" thick	2160	35	Coating failure at 20 sec. some Mo oxidation apparent
Mo with Al-Si flame-sprayed, oxidized coating, .010" thick	2160	35	Coating failure at 28 sec. with oxidation of Mo apparent
Mo with W-2 vapor-deposited coating, .0014" thick	1880	37	Full size probe. Excellent preservation of probe tip contour throughout test
Mo with W-2 vapor-deposited coating, .0014" thick	2180	40	Coating failure at 22 sec. Catastrophic oxidation of Mo apparent at 27 sec.
Mo with LM-5 flame-sprayed coating, .015" thick	2110	32	Rapid flaking of coating at 22 sec. Catastrophic oxidation of Mo evident
Graphite with SiC vapor-deposited coating, .010" thick	1840	38	Excellent preservation of probe tip contour throughout test
Graphite with Am. Lava coating, .005" thick	2075	35	Slight oxidation and erosion apparent at 26 sec.
Graphite with $90W+10ZrO_2$ Flame-sprayed coating, .015" thick	2260	35	Coating failure on rim at 25 sec. Slight erosion apparent

The above results show that one model with a W-2 coating and another with a $MoSi_2$ coating withstood the heat inputs well; whereas, other probes having identical coatings exhibited poor heat resistance. These discrepancies in performance were attributed to differences in quality or workmanship of the

coatings. Other coatings that failed, stripped or flaked-off within 35 seconds as a result of brittleness or poor erosion and thermal shock resistance. The main causes for poor heat resistances of the uncoated models were melting, erosion and oxidation.

Although subjected to the same heat inputs, the maximum surface temperatures at the tips of the models varied considerably. These variances were due to the different emissivities, decomposition rates, densities, thermal conductivities and heat capacities of the various materials and coatings. A molybdenum probe with a zirconium diboride (ZrB_2) coating attained the highest surface temperature, 2325°C (4215°F), due to lower thermal conductivity and less heat capacity compared with most of the other coatings.

METALLURGICAL EXAMINATIONS:

Heat effects on the electric arc-tested probes, which were determined by visual or macroscopic examinations at magnifications up to 10 times, are shown in Figures 5 and 6. The results from these examinations and subsequent microscopic examinations at magnifications up to 1000 times corroborated the results previously disclosed by observations of the color motion pictures taken during the electric arc heat tests. These results are shown below.

COATED MOLYBDENUM PROBES:

Out of nine oxidation-resistant coatings tested on molybdenum, the first probe model, Figure 5, which had a 90% tungsten + 10% zirconia coating exhibited the least damage. Subsequent microscopic examination disclosed that, except for some slight oxidation and erosion, this coating had virtually remained intact with no apparent damage to the base metal, as shown on the photomicrographs in Figure 7. The next four molybdenum probes (Fig.5) containing aluminum-chromium-silicon, gradated zirconia, zirconium and molybdenum disilicide coatings exhibited about the same degree of damage. These probes were slightly eroded and some oxidation products in powder form had redeposited at the rear. Even though the gradated zirconia coating on the molybdenum was cracked and had flaked-off somewhat at the leading edge radius, this model had still maintained its basic configuration. Subsequent microscopic examination revealed that the metal-rich undercoat remained intact and evidently was able to protect the base metal from catastrophic oxidation.

As previously mentioned, one molybdenum probe with a molybdenum disilicide ($MoSi_2$) coating and another full-size probe with a W-2 coating performed well. On the other hand, another probe model with an identical $MoSi_2$ coating exhibited a considerable amount of scaling at the nose tip and pressure cavity. The other model with an identical W-2 coating as the full-size probe showed visible evidences of scaling and catastrophic oxidation. These discrepancies were evidently due to differences in the quality or workmanship of the coatings. According to the findings of others (5), the capability of a coating is dependent on its quality structure of the coatings before and after the heat tests are shown in Figures 7 thru 16. The coatings which performed poorly were found to be blistered and contained numberous microcracks prior to being subjected to the heat tests. These defects were found by examining flat specimens having

these identical coatings. No microscopic examination was made on the full-size probe with the W-2 coating which performed well. This probe was coated at a later date than the probe model which performed poorly and therefore, probably did not contain any microcracks or other detrimental defects. This improvement was most likely due to optimization in the quality or workmanship of the W-2 coating (5). $MoSi_2$ and W-2 coatings are vapor-deposited coatings that contain certain amounts of silicon. Other molybdenum probes with vapor-deposited and/or silicon-bearing coatings, such as DURAK-MG, aluminum-silicon (AL-Si) and LM-5 coatings also exhibited visible evidences of scaling at the nose tips and pressure cavities. No microcracks were visilbe upon microscopic examination of flat specimens having these identical coatings. Since it was impossible to examine all areas of the coatings microscopically, microcracks could still have been present in the coatings before the heat tests. Thermal cracks could develop during the heat tests which would cause subsequent scaling and oxidation of the exposed surface of the base metal. In addition to thescaling, the model with the LM-5 had oxidized catastrophically. This was attributed to the poor mechanical bond between the coating and the base metal, as shown in Figure 8.

COATED GRAPHITE PROBES:

Metallurgical examination of three graphite probes with oxidation-resistant coatings disclosed that the probe with the self-bonded, silicon carbide (SiC) coating exhibited the least damage (slight erosion), as shown in Figure 6. This model, however, fractured when accidently dropped during transportation. Microscopic examination revealed that this probe was virtually unaffected by the heac test as shown in Figure 17. The other two models containing the 90% tungsten + 10% zirconia (Fig. 18) and the Am Lava coatings (Fig.19) exhibited about the same degree of erosion and oxidation damage. As previously mentioned, the graphite probe with the 90W + $10Z_rO_2$ coating broke at the threads when swung out of the arc. This susceptibility to fracturing at such low stress values indicates that graphite, by itself, is too brittle at low temperatures to be a suitable, basic probe material.

CONCLUSIONS:

1. Molybdenum when adequately protected against oxidation was found to be superior to graphite for structural use on the probe.

2. The 90%W + 10% Z_rO_2, flame-sprayed coating was the best coating tested for use on a molybdenum probe.

3. Al-Cr-Si, M_oS_{i2}, gradated zirconia, and Z_rO_2 coatings on molybdenum were slightly inferior to the above coating.

4. Self-bonded, vapor-deposited silicon carbide coating was the best coating tested for use on a graphite probe.

5. American Lava Corp. coating and a 90%W + 10% Z_rO_2 flame-sprayed coating on graphite eroded, but still offered protection against oxidation of the graphite.

6. The following silicon-bearing and/or vapor-deposited coatings on molybdenum were subject to scaling of the nose tip and pressure cavity:

a. Durak - Mg
b. W-2
c. Al-Si, oxidized
d. LM-5

7. Optimization and improvement in the quality and workmanship of the W-2 and $M_oS_{i_2}$ coatings were evidently the reasons for improved performances of these coatings.

8. Although subjected to the same heat inputs, the maximum observed surface temperatures on the models varied considerably from 1790°C (3255°F) to 2325°C (4215°F). This variance was attributed to the different emissivities, thermal conductivities, heat capacities, decompositon rates and densities of the various coatings and materials.

9. Vapor-deposited coatings exhibited excellent metallurgical or chemical bonds between the coatings and the base metals; whereas, flame-sprayed coatings contained poor to good mechanical or mechanical-chemical bonds.

10. The effects of a slight amount of ablation, deformation, erosion or deposit on the nose tip of the probe on the efficiency of the probe should be investigated.

REFERENCES:

1. Stewart, J. D., "Estimated Fluxes on Proposed Pitot Tubes for Testing in Water-Arc", General Electric Co. (MSVD), Phila., May, 1959, Internal Report No. AT117-91.

2. Dank, Nelson, Sheridan and Sutton, "Water Stabilized Arc Tests on Nonmetallic Materials", Journal of the Electrochamical Soc., April, 1959, Vol. 106, No. 4.

3. Molella, J. P., "Investigation and Evaluation of Available Hypersonic Probe Materials and Oxidation-Resistant Coatings for Possible Use at 4000°F for 60 Seconds", Picatinny Arsenal, Dec., 1959, TM No. ME-5-59.

4. Smithells, Metals Reference Book, Interscience Publishers Inc., N. Y., 1955, Vol. II, P. 662.

5. Wilkes, Charles, and Magalotti, "Evaluation of Coatings for Molybdenum", June 1961, Final Report under Contract NOw 60-0321c.

6. Chromalloy Corp., "Development of a Powder and/or Gas Cementation Process for Coating Molybdenum Alloys for High Temperature Protection", Preliminary Information Under an Air Force Contract.

FIGURES 1 through 19

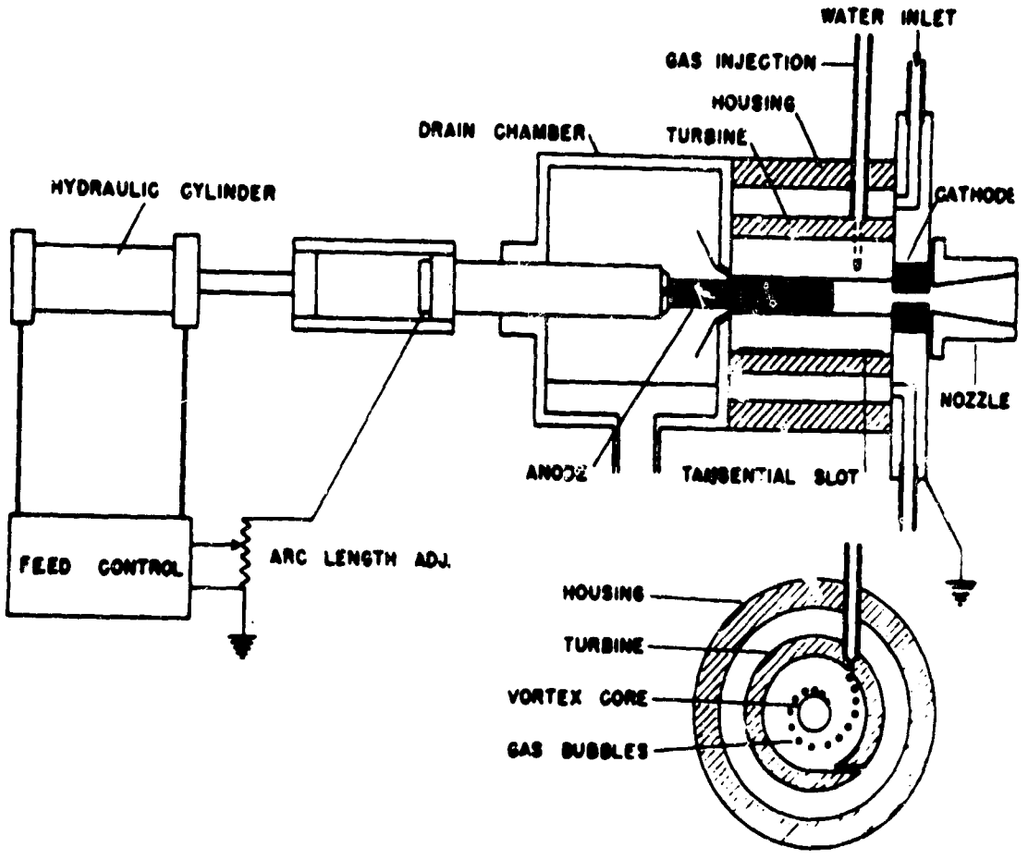

Figure I. Schematic diagram of water-stabilized electric arc

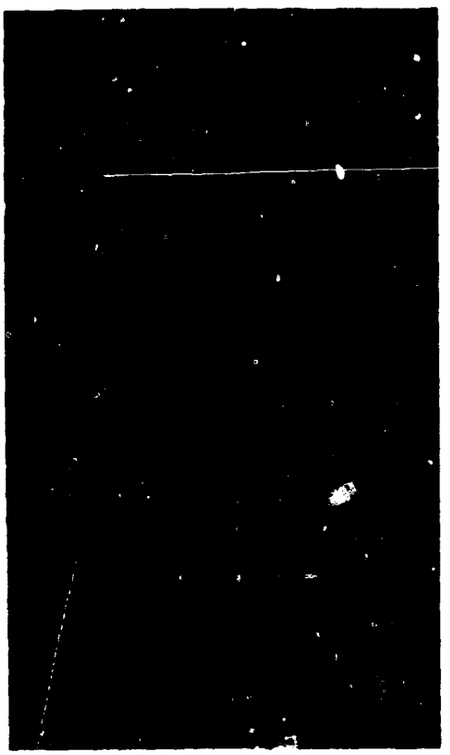

Figure 2. Water-stabilized electric arc apparatus before operation.

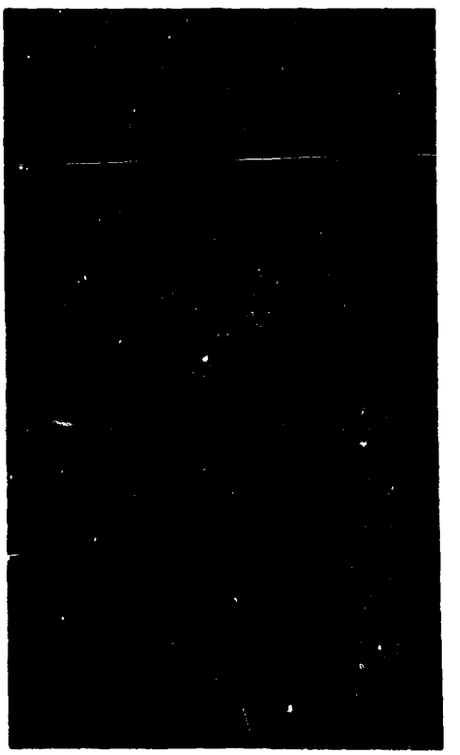

Figure 3. Electric arc during operation.

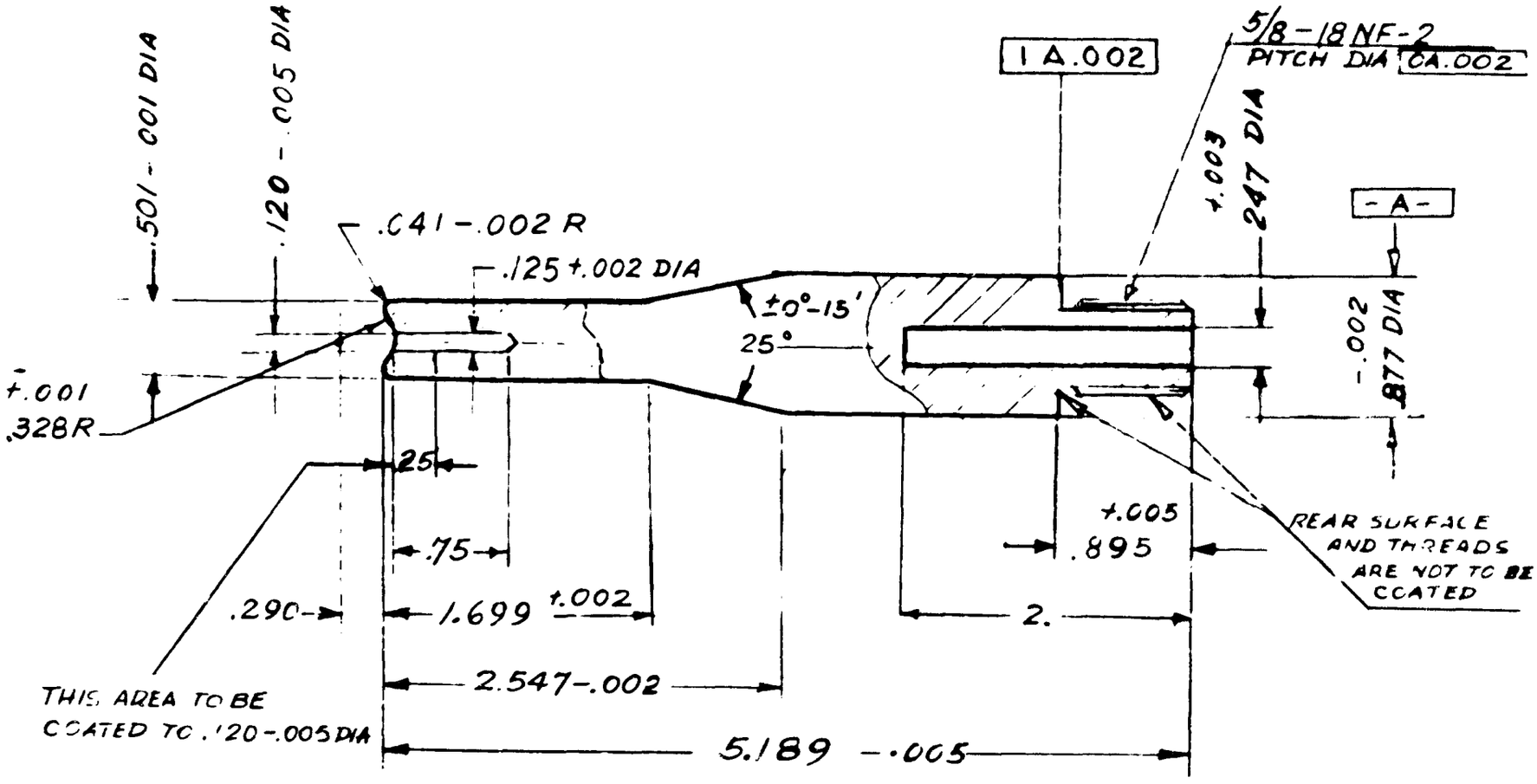

NOTE: FINISH ALL OUTSIDE SURFACES AFTER COATING

FIGURE 4
PROBE EXPERIMENTAL

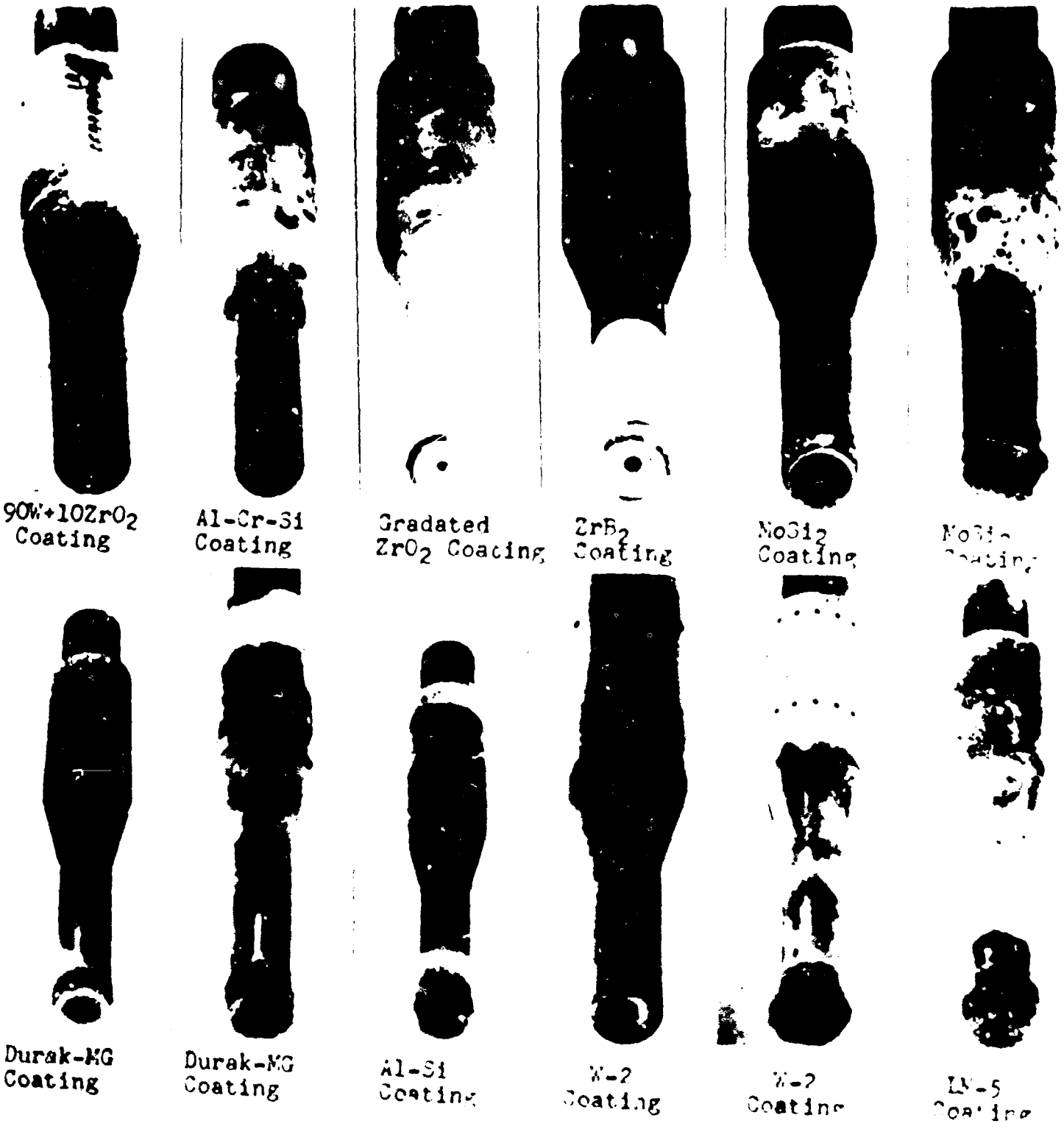

Figure 5 Photographs of molybdenum arc-tested probes with various protective coatings.

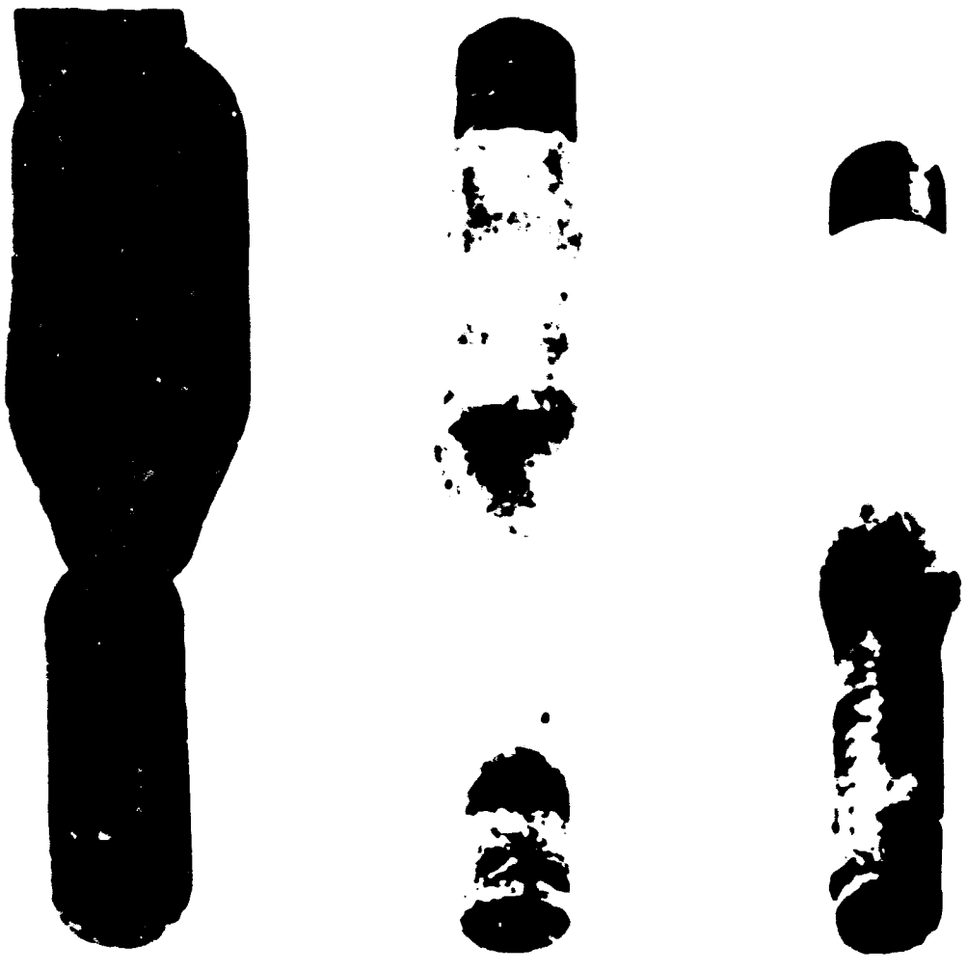

Graphite w/ SiC Coating

Figure 6

A

Before Plasma-Arc Jet test. Note slight porosity of cermet coating and excellent mechanical bond at interface.

1. Cermet (90% W+10% $Zr^{0}2$) coating
2. Porosity
3. Interface
4. Base metal

B

After Plasma-Arc Jet test 0.50 inch from nose tip. Note very slight erosion and/or sublimation of coating. Interface and base metal remained intact.

1. Coating
2. Erosion and/or sublimation
3. Interface
4. Base metal

C

After Plasma-Arc Jet test at nose tip. Note that traces of eroded, sublimed and oxidized coating still remain. Also note that base metal was not affected.

1. Coating
2. Eroded, sublimed and oxidized areas
3. Base metal

Figure 7 Microstructure of Linde LW-6Z10 Cermet (90% W+10% Zr^{0}_{2}) coating on Molybdenum.
Etchant - NaOH + $K_3Fe(CN)_6$ Magnification - 1000X

A

Before Plasma-Arc Jet test. Note wide interfacial zone and good bond between coating and base metal at interface.

1. Coating
2. Interfacial zone
3. Interface
4. Base metal

B

After Plasma-Arc Jet test 0.50 inch from nose tip. Note erosion of coating and slight oxidation along interface. Interfacial zone and base metal remained relatively intact.

1. Eroded coating
2. Interfacial zone
3. Oxidized interface
4. Base metal

C

After Plasma-Arc Jet test at nose tip. Note that coating was almost completely eroded away and that base metal was eroded and slightly oxidized at the surface.

1. Remainder of eroded coating
2. Eroded and slightly oxidized surface of base metal
3. Base metal

Figure 8 Microstructure of Aluminum-Chromium-Silicon coating on Molybdenum
Etchant - NaOH + $K_3Fe(CN)6$
Magnified - 1000X

A 100X

Photomicrograph at low magnification showing metal-rich undercoat and ceramic-rich overcoat.

1. Ceramic-rich overcoat
2. Metal-rich undercoat
3. Base metal

B 1000X

Photomicrograph at high magnification taken at interface of base metal and undercoat. Note excellent bond at interface and slight porosity of undercoat.

1. Undercoat
2. Porosity
3. Interface
4. Base metal

C 1000X

Photomicrograph at high magnification taken at interface of undercoat and overcoat. Note poor bond at interface.

1. Overcoat
2. Interface
3. Undercoat

Figure 9 Microstructure of gradated Zirconia coating on Molybdenum before Plasma-Arc Jet test. Etchant - NaOH + $K_3Fe(CN)6$

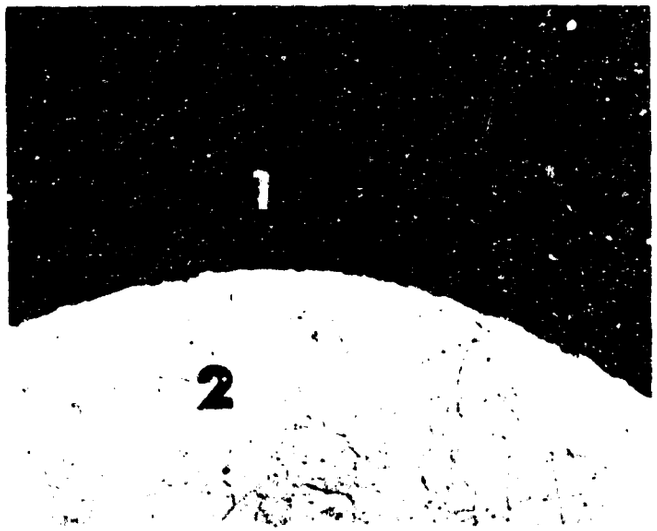

A 100X

Photomicrograph of nose tip radius. Note complete removal of overcoat and oxidation and erosion of undercoat. Also note that base metal remained intact.

1. Undercoat
2. Base metal

B 100X

Photomicrograph taken 0.50 inch from nose tip. Note open crack at overcoat and porosity at interface between overcoat and undercoat. Base metal remained intact.

1. Overcoat
2. Open crack
3. Porosity at interface
4. Undercoat
5. Base metal

Figure 10 Microstructure of gradated Zirconia on Molybdenum after Plasma-Arc Jet test. Etchant - $NaOH + K_3Fe(CN)6$

A

Before Plasma-Arc Jet Test. Note good mechanical bond between coating and base metal. Also, note slight porosity of coating and interface.

1. Coating
2. Interface
3. Porosity
4. Base metal

B

After Plasma-Arc Jet Test 0.50 inch from nose tip. Note cracking of coating and oxidation of interface with no apparent damage of base metal.

1. Coating
2. Crack
3. Oxidation of interface
4. Base metal

C

After Plasma-Arc Jet Test at nose tip. Note erosion of coating and oxidation of interface and no apparent damage of base betal.

1. Coating
2. Eroded area
3. Oxidized interface
4. Base metal

Figure 11 Microstructure of Zirconium Diboride Coating on Molybdenum. Etchant - $NaOH + K_3Fe(CN)_6$

Magnification - 1000X

A 1000X

Before Plasma-Arc Jet test. Note excellent metallurgical bond at very thin interfacial zone.

1. Coating
2. Interfacial zone
3. Base metal

B 1000X

After Plasma-Arc Jet test 0.50 inch from nose tip. Note growth of interfacial zone and also note that coating and base metal remained intact.

1. Coating
2. Interfacial zone
3. Base metal

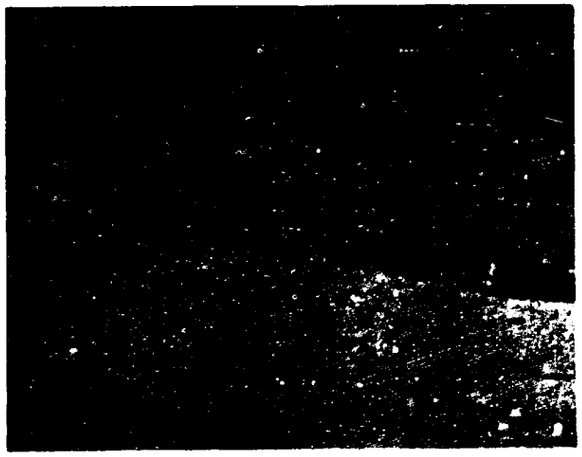

C 250X

After Plasma-Arc Jet test at nose tip. Note uniform oxidation of base metal and slight amount of floating of base metal to the surface.

1. Oxidation
2. Floated base metal
3. Base metal

Figure 12 Microstructure of Molybdenum Disilicide coating on molybdenum +0.5% of Titanium alloy. Etchant - NaOH + $K_3Fe(CN)6$

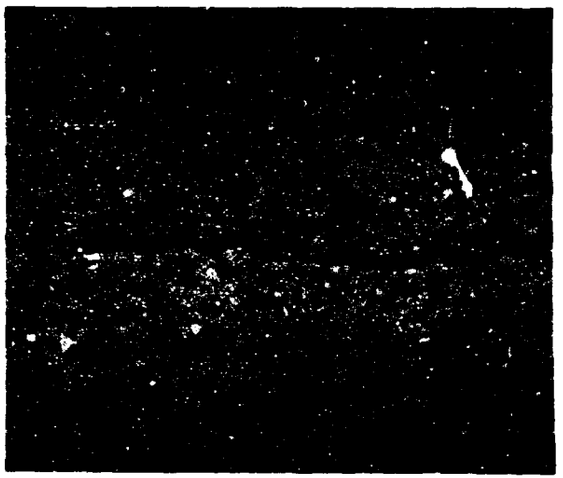

A 1000X

Before Plasma-Arc Jet test.Note very wide interfacial zone and equi-axed, fine-grained structure of coating.

1. Coating
2. Interfacial zone
3. Base metal

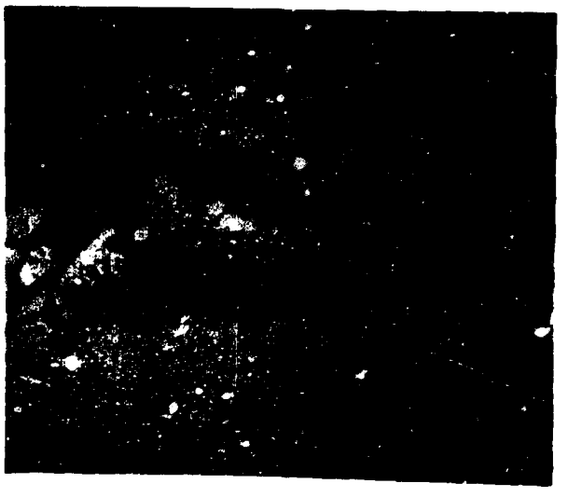

B 250X

After Plasma-Arc Jet Test 0.50 inch from nose tip. Note oxidation of coating and interface and floating of coating and base metal to the oxide.

1. Oxide
2. Floated metal
3. Interface
4. Base metal

C 250X

After Plasma-Arc Jet test at nose tip. Note uniform oxidation of base metal and cracking of oxide.

1. Oxide
2. Cracks
3. Base metal

Figure 13 Microstructure of DURAK-MG coating on molybdenum. Etchant - $NaOH + K_3Fe(CN)6$

A

Before Plasma-Arc Jet test. Note complex interfacial zone and equi-axed grain structure of coating.

1. Coating
2. Interfacial zone
3. Base metal

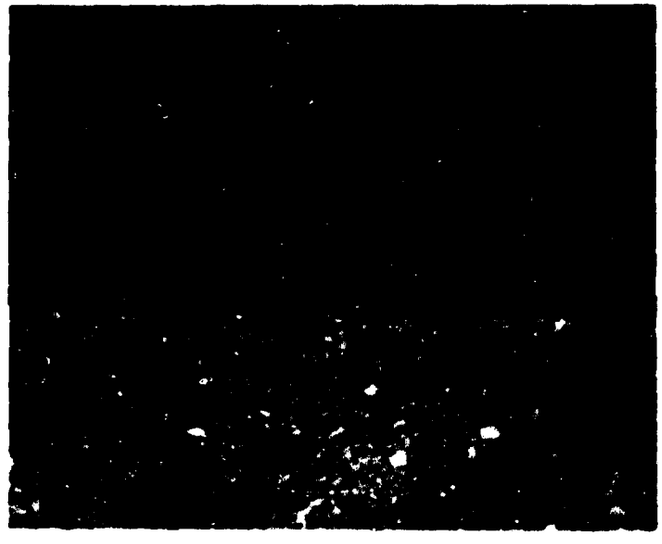

B

After Plasma-Arc Jet test. Representative microstructure at and 0.50 inch from nose tip. Note uniform oxidation of the base metal and slight traces of metallic coating.

1. Oxide
2. Traces of metallic coating
3. Base metal

Figure 14 Microstructure of Aluminum Silicon Oxidized coating on molybdenum.
Etchant - NaOH + $K_3Fe(CN)6$ Magnification - 1000X

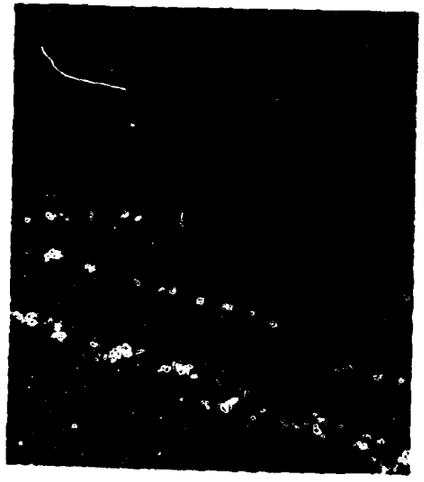

A

Before Plasma-Arc Jet test. Note cracking and columnar structure of coating and thin interfacial zone.

1. Coating
2. Interfacial zone
3. Base metal

B

After Plasma-Arc Jet test 0.50 inch from nose tip. Note oxidation of coating and base metal and floating of coating to the oxide surface.

1. Oxide
2. Coating
3. Base metal

C

After Plasma-Arc Jet test at nose tip. Note lack of coating, catastrophic oxidation of base metal and floating of base metal tothe oxide surface.

1. Oxide
2. Floated base metal
3. Base metal

Figure 15 Microstructure of Chromalloy W-2 coating on molybdenum
Etchant - NaOH + $K_3Fe(CN)6$ Magnification - 1000X

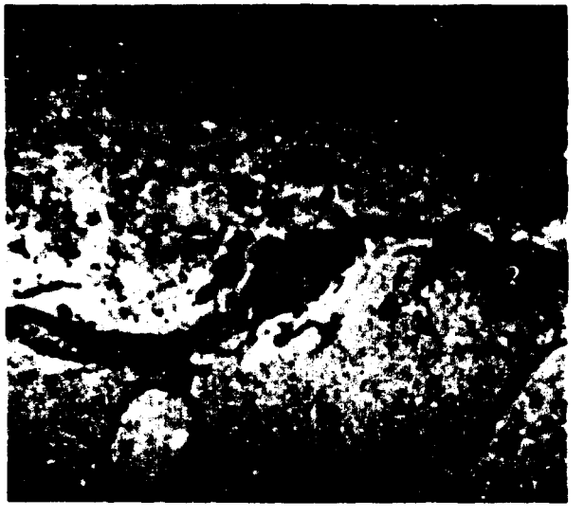

A

Before Plasma-Arc Jet test. Note slight porosity at coating and interface and mechanical bond at interface.

1. Coating
2. Porosity
3. Interface
4. Base metal

B

After Plasma-Arc Jet test 0.50 inch from nose tip. Note oxidation and melting of coating and base metal.

1. Coating
2. Base metal

C

After Plasma-Arc Jet test at nose tip. Note irregular catastrophic oxidation of the base metal and floating of the base metal to the surface.

1. Oxide
2. Floated base metal
3. Base metal

Figure 16 Microstructure of Linde LM-5 coating on Molybdenum
Etchant - NaOH + $K_3Fe(CN)6$

Magnification - 1000X

A 1000X

Before Plasma-Arc Jet test. Note dense coating and excellent chemical bond at interface. Also note porosity of base material.

1. Coating
2. Interface
3. Base material

B 100X

After Plasma-Arc Jet test 0.50 inch from nose tip. Note that thin layer of sublimed coating still remains. Base material was only slightly eroded at surface.

1. Thin layer of coating
2. Slightly eroded base material
3. Base material

C 100X

After Plasma-Arc Jet test at nose tip. Note that slight traces of sublimed coating still remain. Also note eroded surface of base material.

1. Traces of coating
2. Eroded surface of base material
3. Base material.

Figure 17 Structure of Crystolon "C" self-bonded Silicon Carbide coating on graphite. Unetched

A

Before Plasma-Arc Jet Test. Note excellent bonding of coating to base material. Also note porosity of base material

1. Coating
2. Porosity
3. Base material

B

After Plasma-Arc Jet Test 0.50 inch from nose tip. Note oxidation and/or erosion of surface of coating.

1. Oxidation and/or erosion
2. Coating
3. Base material

C

After Plasma-Arc Jet Test. Note erosion of base material and traces of coating.

1. Erosion of base material
2. Coating
3. Base material

Figure 18 Microstructure of American Lava coating on graphite.
Unetched

Magnification - 250X

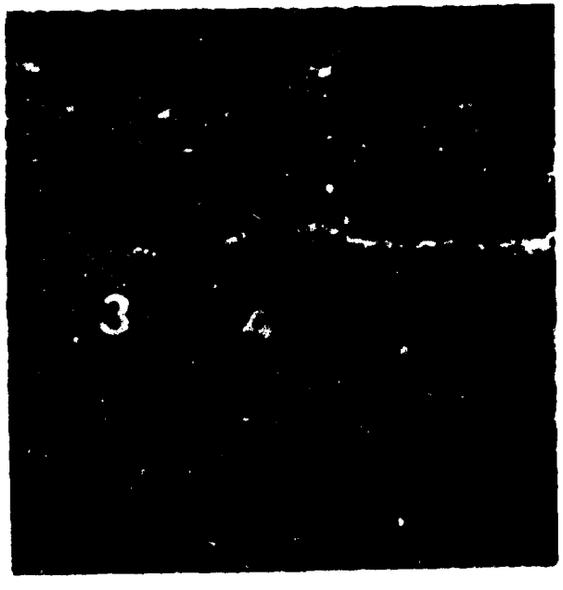

A

Unetched 250X

Before Plasma-Arc Jet test. Note excellent bond of tantalum undercoat and Linde LW-6Z10 overcoat and porosity of base material.

1. Overcoat
2. Undercoat
3. Base material
4. Porosity

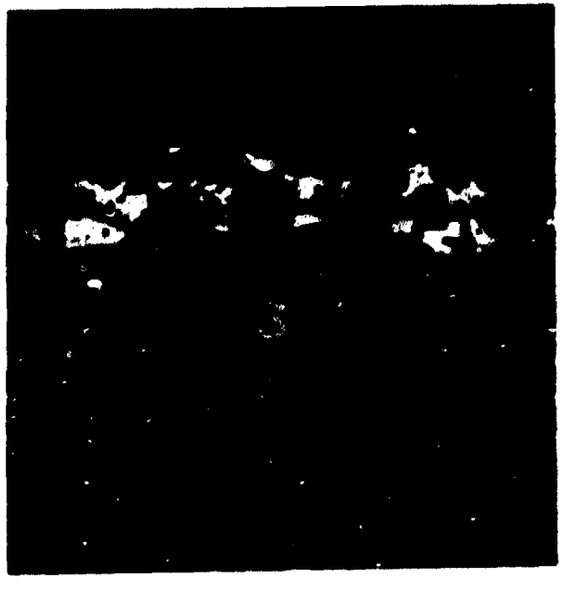

B

Unetched 500X

After Plasma-Arc Jet test. Representative structure at and 0.50 inch from nose tip. Note complete oxidation of remainder of overcoat and undercoat. Base material remained intact.

1. Complete oxidation of overcoat
2. Partial oxidation of overcoat and undercoat.
3. Base material

Figure 19 Structure of Linde LW-6Z10 coating on graphite.